Nuclear Engineering and Technology 52 (2020) 1443–1451

Contents lists available at ScienceDirect

Nuclear Engineering and Technology

journal homepage: www.elsevier.com/locate/net

Original Article

Robust power control design for a small pressurized water reactor using an *H* infinity mixed sensitivity method

Xu Yan, Pengfei Wang*, Junyan Qing, Shifa Wu, Fuyu Zhao

School of Nuclear Science and Technology, Xi'an Jiaotong University, Xi'an, 710049, China

ARTICLE INFO

Article history:
Received 9 January 2019
Received in revised form
31 December 2019
Accepted 31 December 2019
Available online 2 January 2020

Keywords:
Reactor power
Multimodel
H_∞ mixed sensitivity
Robust control

ABSTRACT

The objective of this study is to design a robust power control system for a small pressurized water reactor (PWR) to achieve stable power operations under conditions of external disturbances and internal model uncertainties. For this purpose, the multiple-input multiple-output transfer function models of the reactor core at five power levels are derived from point reactor kinetics equations and the Mann's thermodynamic model. Using the transfer function models, five local reactor power controllers are designed using an *H* infinity (H_∞) mixed sensitivity method to minimize the core power disturbance under various uncertainties at the five power levels, respectively. Then a multimodel approach with triangular membership functions is employed to integrate the five local controllers into a multimodel robust control system that is applicable for the entire power range. The performance of the robust power system is assessed against 10% of full power (FP) step load increase transients with coolant inlet temperature disturbances at different power levels and large-scope, rapid ramp load change transient. The simulation results show that the robust control system could maintain satisfactory control performance and good robustness of the reactor under external disturbances and internal model uncertainties, demonstrating the effective of the robust power control design.

1. Introduction

The small pressurized water reactor (PWR) has the advantages of good economy and high safety, which is currently one of the research focuses in the field of nuclear energy [1]. Compared with large reactors, small PWRs not only have flexible operating conditions, but also process fast and deep load-follow capability. Operating conditions of the small PWRs implementing in floating power stations are often more complex than land-based large reactors due to strong external disturbances and internal uncertainties. These uncertainties and external factors make it difficult to control the reactor power of small PWRs.

The reactor core is the site where fission reactions occur in nuclear reactors. Changes in reactor core parameters and external environmental disturbances will lead to neutron flux density changes, making rapid power changes and endangering reactor safety [2]. Therefore, a core power controller in actual operation condition is designed to ensure the safety and stability of a reactor. Due to the uncertainties of small PWRs and strong external disturbances, the classical control method is hard to achieve good control of reactor core power during entire operational conditions, while the robust control based on the modern control theory is an effective method. At present, a lot of researches focusing on robust reactor power control have been carried out. Liu et al. [3] designed a fuzzy robust controller for nuclear reactor power based on a T-S fuzzy model. Wu [4]. designed a robust reactor power control system based on the quantitative feedback theory (QFT). Li et al. [5,6] designed a LQG/LTR robust controller for load-follow control of PWRs. Ansarifar et al. [7] used the sliding-mode observer to estimate the xenon concentration in a reactor core, and designed a robust reactor power controller based on the sliding-mode control. Liao et al. [8] used an internal model robust control method to design the reactor power control system of a small PWR. Zaidabadi et al. [9] designed the feedback-linearization control for axial power distribution in pressurized water reactors during load-following operations. Mousakazemi et al. [10] used a robust Proportional-Integral-Derivative (PID) controller optimized by the particle swarm optimization for reactor power control.

Among various robust control methods, the H infinity (H_∞) robust control method take into full account the uncertainty of a control object, which is suitable for complex systems with external

* Corresponding author.
E-mail address: wangpengfei@xjtu.edu.cn (P. Wang).

https://doi.org/10.1016/j.net.2019.12.031

Nomenclature

n_r	Relative neutron density
c_r	Relative density of the delayed neutron precursor
ρ	Total reactivity
ρ_{rod}	Reactivity contributed by control rods
β	Delayed neutron fraction
λ	Decay constant of the delayed neutron precursor, s^{-1}
α_f	Fuel reactivity temperature coefficient, $^\circ C^{-1}$
α_c	Coolant reactivity temperature coefficient, $^\circ C^{-1}$
Λ	Average neutron generation time,s
f	Fraction of the core power generated in the fuel
T_f	Average temperature of the fuel, $^\circ C$
T_{c1}	Outlet temperature of the coolant node 1, $^\circ C$
T_{c2}	Outlet temperature of the coolant node 2, $^\circ C$
T_{lp}	Coolant inlet temperature, $^\circ C$
Ω	Heat transfer coefficient between the fuel and coolant, $W/^\circ C$
μ_f	Total heat capacity of fuel, $J/^\circ C$
μ_c	Total heat capacity of coolant, $J/^\circ C$
P_0	Reactor full power, W
T_{f0}	Initial temperature of T_f $^\circ C$
$T_{c1,0}$	Initial temperature of T_{c1}, $^\circ C$
$T_{c2,0}$	Initial temperature of T_{c2}, $^\circ C$
δ	Deviation of a variable from an equilibrium value
$r(t)$	Reference input
$e(t)$	Tracking error
$u(t)$	Control input
$d(t)$	Disturbance parameter
$y(t)$	System output
$K(s)$	Controller
$G(s)$	Controlled object model
$W_1(s)$	Weight function of $e(t)$
$W_2(s)$	Weight function of $u(t)$
$W_3(s)$	Weight function of $y(t)$
z_1	Signal for $W_1(s)$
z_2	Signal for $W_2(s)$
z_3	Signal for $W_3(s)$
$S(s)$	Sensitivity function
$R(s)$	Control sensitivity function
$T(s)$	Complementary sensitivity function
G_{ci}	Reactor power controller
K_c	Transfer function of the control rod drive mechanism
K_r	Control rod differential worth
$H(s)$	Transfer function of nuclear power measuring equipment
$G_{c,m}$	Multi-model robust power controller

disturbances and model uncertainties [11]. Therefore, many scholars have studied the H_∞ robust control of reactor core power and made comparative analysis of it with other control methods. Suzuki et al. [12] designed a reactor core power control system based on the H_∞ robust control method. Simulation results have demonstrated that it has stronger stability robustness and anti-interference robustness compared with that based on the LQG robust control method. Chi et al. [13] applied the optimal control theory of H_∞ to the xenon poison control in a PWR core, and compared the robust control effect of the H_∞ with that of the LQG, which shows that the gain and phase margins under the H_∞ robust control were much larger than those under the LQG robust control. Sun et al. [14] designed the H_∞ robust power control system for a reactor, and proved that its control performance is superior to that of the traditional proportional-integral-derivative (PID) based control system. These H_∞ robust power controllers are all designed based on the linearized reactor core model at the 100% of full power (FP), so they are expected to have satisfactory control performance only in a limited power range around the 100% FP. Therefore, they usually do not have good control performance or are even ineffective, when the reactor power is often under dramatic changes in a wide range.

Nowadays, many scholars in their professional fields are still illustrating the superiority of H_∞ control in the latest literatures. Sedhon et al. [15] introduced the H_∞ control method to adjust microgrids voltage and frequency, and the simulation results showed that it is better than the drop controller in terms of the current waveform. In the field of switched reluctance machines, Rigators et al. [16] designed an H_∞ controller, and also it has better anti-disturbance ability than the PID controller and the back-stepping controller. Madhavi et al. [17] applied an H_∞ control method to the converter for fuel cell applications. And it has been demonstrated that the H_∞ control method possesses less rising time and setting time for the converter compared with the current mode control method. For the T-S aero-engine wireless network system, Zhou et al. [18] showed that the H_∞ control is better than the Sliding mode control in terms of the network system stability. Tumari et al. [19] presented the H_∞ control for the liquid slosh suppression, and the simulation curves demonstrated that it has shorter setting time and lower overshoot than the Hybrid Fuzzy-PIDF controller.

Based on the analysis above, the robust control of reactor core power in a small PWR is studied based on the H_∞ hybrid sensitivity control theory and a multi-model approach. Considering the uncertainties of the reactor core model in a wide power range, a multi-model reactor core system is established for all operational conditions, based on which a multi-model H_∞ robust control system is designed to achieve satisfactory control of the reactor power for all operational conditions.

2. Reactor core model

The reactor core model consists of the point kinetics equations with one group delayed neutron and reactivity feedbacks due to

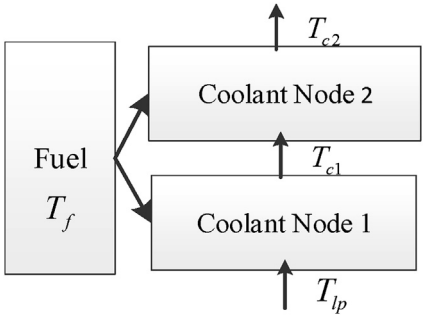

Fig. 1. The relationship between fuel and coolant nodes.

changes in fuel and coolant temperatures, as well as the core thermal dynamic equations developed based on the Mann's model with one fuel node and two coolant nodes in Fig. 1 [20].

2.1. Nonlinear model

The nonlinear reactor core model described by a set of first-order ordinary equations can be given as [21].

$$\begin{cases} \dfrac{dn_r}{dt} = \dfrac{\rho-\beta}{\Lambda} n_r + \lambda c_r \\ \dfrac{dc_r}{dt} = \dfrac{\beta}{\Lambda} n_r - \lambda c_r \\ \mu_f \dfrac{dT_f}{dt} = f P_0 n_r - \Omega\left(T_f - T_{c1}\right) \\ \dfrac{\mu_c}{2}\dfrac{dT_{c1}}{dt} = \dfrac{1}{2}\left[(1-f)P_0 n_r + \Omega\left(T_f - T_{c1}\right)\right] + C_{pc} W_p \left(T_{lp} - T_{c1}\right) \\ \dfrac{\mu_c}{2}\dfrac{dT_{c2}}{dt} = \dfrac{1}{2}\left[(1-f)P_0 n_r + \Omega\left(T_f - T_{c2}\right)\right] + C_{pc} W_p (T_{c1} - T_{c2}) \\ \rho = \rho_{rod} + \alpha_f\left(T_f - T_{f,0}\right) + \dfrac{\alpha_c}{2}\left[(T_{c1}+T_{c2}) - (T_{c1,0}+T_{c2,0})\right] \end{cases} \tag{1}$$

where n_r denotes the relative neutron density; c_r denotes the relative density of the delayed neutron precursor; ρ and ρ_{rod} denote the total reactivity and the reactivity introduced by control rods, respectively; β denotes the delayed neutron fraction; λ denotes the decay constant of the delayed neutron precursor, s^{-1}; α_f and α_c denote the reactivity temperature coefficients of the fuel and coolant, respectively, $^\circ C^{-1}$; Λdenotes the average neutron generation time,s; f denotes the fraction of the core power generated in the fuel; T_f denotes the average temperature of the fuel, $^\circ C$; T_{c1} and T_{c2} denote the outlet temperatures of the coolant nodes 1 and 2, respectively, $^\circ C$; T_{lp} denotes the inlet temperature of the coolant nodes 1, $^\circ C$; The relationship between fuel and coolant nodes are illustrated in Fig. 1; Ω denotes the transfer coefficient between the fuel and coolant, $W/^\circ C$; μ_f and μ_c denote the total heat capacities of the fuel and coolant, respectively, $J/^\circ C$; P_0 denotes the reactor full power, W; W_p denotes the coolant flow, kg/s; C_{pc} denotes the specific heat at constant pressure, $J\cdot kg^{-1}\cdot C^{-1}$; T_{f0} denotes the initial temperature of T_f, $^\circ C$; $T_{c1,0}$ denotes the initial temperature of T_{c1}, $^\circ C$; $T_{c2,0}$ denotes the initial temperature of T_{c2}, $^\circ C$.

2.2. Transfer function model

The derivations of n_r, c_i, T_f, T_{c1}, T_{c2} and ρ from their equilibrium values, namely, $n_{r,0}$, $c_{i,0}$, $T_{f,0}$, $T_{c1,0}$, $T_{c2,0}$ and ρ_0, are defined as

$$\begin{cases} \delta n_r = n_r - n_{r,0} \\ \delta c_i = c_i - c_{i,0} \\ \delta T_f = T_f - T_{f,0} \\ \delta T_{c1} = T_{c1} - T_{c1,0} \\ \delta T_{c2} = T_{c2} - T_{c2,0} \\ \delta\rho = \rho - \rho_0 \end{cases} \tag{2}$$

where δ indicates the deviation of a variable from an equilibrium value.

Substituting Eq. (2) into Eq. (1) and ignoring the second-order terms according to the small perturbation linearization methodology, we can finally obtain the following Eqs. (3)–(6) by conducting linearization and Laplace transformation.

$$s\cdot n_r(s) = -\frac{\beta}{\Lambda} n_r(s) + \frac{\beta}{\Lambda} c_r(s) + \frac{\alpha_f n_{r0}}{\Lambda} T_f(s) + \frac{\alpha_c n_{r0}}{2\Lambda} T_{c1}(s) + \frac{\alpha_c n_{r0}}{2\Lambda} T_{c2}(s) + \frac{n_{r0}}{\Lambda}\rho_{rod}(s) \tag{3}$$

$$s\cdot c_r(s) = \lambda(n_r(s) - c_r(s)) \tag{4}$$

$$sT_f(s) = \frac{f_f P_0}{\mu_c} n_r(s) - \frac{\Omega}{\mu_c} T_f(s) + \frac{\Omega}{\mu_f} T_{c1}(s) \tag{5}$$

$$sT_{c1}(s) = \frac{\left(1-f_f\right)P_0}{\mu_c} n_r(s) + \frac{\Omega}{\mu_c} T_f(s) - \left(\frac{\Omega}{\mu_c} + \frac{2M}{\mu_c}\right) T_{c1}(s) + \frac{2M}{\mu_c} T_{lp}(s) \tag{6}$$

$$sT_{c2}(s) = \frac{\left(1-f_f\right)P_0}{\mu_c} n_r(s) + \frac{\Omega}{\mu_c} T_f(s) - \left(\frac{\Omega}{\mu_c} - \frac{2M}{\mu_c}\right) T_{c1}(s) - \frac{2M}{\mu_c} T_{c2}(s) \tag{7}$$

Equations. (3)–(7) can be transformed into a matrix form as

$$A(s)X(s) = B(s)U(s) \tag{8}$$

where X is the state vector and $X(s) = [n_r(s), c_r(s), T_f(s), T_{c1}(s), T_{c2}(s)]^T$; U is the input vector and $U(s) = [\rho_{rod}(s), T_{lp}(s)]^T$; matrixes $\boldsymbol{A}$ and $\boldsymbol{B}$ can be expressed as

$$\mathrm{A} = \begin{bmatrix} \left(s+\frac{\beta}{\Lambda}\right) & -\frac{\beta}{\Lambda} & \frac{-n_{r0}\alpha_f}{\Lambda} & \frac{-n_{r0}\alpha_c}{2\Lambda} & \frac{-n_{r0}\alpha_c}{2\Lambda} \\ \lambda & -(s+\lambda) & 0 & 0 & 0 \\ \frac{f_f P_0}{\mu_f} & 0 & -\left(\frac{\Omega}{\mu_f}+s\right) & \frac{\Omega}{\mu_f} & 0 \\ \frac{\left(1-f_f\right)P_0}{\mu_c} & 0 & \frac{\Omega}{\mu_c} & -\left(\frac{\Omega+2M}{\mu_c}+s\right) & 0 \\ \frac{\left(1-f_f\right)P_0}{\mu_c} & 0 & \frac{\Omega}{\mu_c} & -\frac{\Omega-2M}{\mu_c} & -\left(\frac{2M}{\mu_c}+s\right) \end{bmatrix}$$

$$B^T = \begin{bmatrix} \frac{n_{r0}}{\Lambda} & 0 & 0 & 0 & 0 \\ 0 & 0 & 0 & \frac{-2M}{\mu_c} & 0 \end{bmatrix}$$

From Eqs. (3)–(8), we can obtain

$$\begin{bmatrix} \delta n_r(s) \\ \delta T_{c2}(s) \end{bmatrix} = \begin{bmatrix} G_{11}(s) & G_{12}(s) \\ G_{21}(s) & G_{22}(s) \end{bmatrix} \begin{bmatrix} \delta\rho_{rod}(s) \\ \delta T_{lp}(s) \end{bmatrix} \tag{9}$$

where transfer functions $G_{11}(s)$, $G_{12}(s)$, $G_{21}(s)$ and $G_{22}(s)$ at the 100%, 80%, 60%, 40% and 20% of full power for the small PWR in the present study are calculated as Eqs. (10)-(14).

$$\begin{bmatrix} G_{11}=\dfrac{10^4\times\left(5.25s^4+57.62s^3+186.6s^2+153.7s+10.76\right)}{s^5+377s^4+4099s^3+14330s^2+17380s+579} & G_{12}=\dfrac{-77.7s^3-765.2s^2-1000s-72.51}{s^5+377s^4+4099s^3+14330s^2+17380s+579} \\ G_{21}=\dfrac{10^4\times\left(5.706s^3+202.2s^2+1367s+104.1\right)}{s^5+377s^4+4099s^3+14330s^2+17380s+579} & G_{22}=\dfrac{17.52s^3+6354s^2+8142s-122.7}{s^5+377s^4+4099s^3+14330s^2+17380s+579} \end{bmatrix} \tag{10}$$

$$\begin{bmatrix} G_{11}=\dfrac{10^4\times\left(5.25s^4+57.51s^3+186.s^2+153.1s+10.71\right)}{s^5+377s^4+4077s^3+13970s^2+15800s+461.8} & G_{12}=\dfrac{-77.55s^3-762.5s^2-996.3s-72.23}{s^5+377s^4+4077s^3+13970s^2+15800s+461.8} \\ G_{21}=\dfrac{10^4\times\left(4.556s^3+161.3s^2+1090s+82.95\right)}{s^5+377s^4+4077s^3+13970s^2+15800s+461.8} & G_{22}=\dfrac{17.45s^3+6348s^2+8433s-97.43}{s^5+377s^4+4077s^3+13970s^2+15800s+461.8} \end{bmatrix} \tag{11}$$

$$\begin{bmatrix} G_{11}=\dfrac{10^4\times\left(5.25s^4+57.48s^3+185.6s^2+152s+10.63\right)}{s^5+377s^4+4060s^3+13620s^2+14170s+344.3} & G_{12}=\dfrac{-77.7s^3-764.7s^2-989s-71.66}{s^5+377s^4+4060s^3+13620s^2+14170s+344.3} \\ G_{21}=\dfrac{10^4\times\left(3.424s^3+120.2s^2+810.6s+61.71\right)}{s^5+377s^4+4060s^3+13620s^2+14170s+344.3} & G_{22}=\dfrac{17.56s^3+6404s^2+8688s-71.81}{s^5+377s^4+4060s^3+13620s^2+14170s+344.3} \end{bmatrix} \tag{12}$$

$$\begin{bmatrix} G_{11}=\dfrac{10^4\times\left(5.25s^4+57.25s^3+183.8s^2+148.7s+10.39\right)}{s^5+376.9s^4+4028s^3+13170s^2+12380s+225} & G_{12}=\dfrac{-77.7s^3-763.4s^2-967.9s-70.04}{s^5+376.9s^4+4028s^3+13170s^2+12380s+225} \\ G_{21}=\dfrac{10^4\times\left(2.283s^3+78.8s^2+528.2s+40.21\right)}{s^5+376.9s^4+4028s^3+13170s^2+12380s+225} & G_{22}=\dfrac{17.62s^3+6444s^2+8805s-46.09}{s^5+376.9s^4+4028s^3+13170s^2+12380s+225} \end{bmatrix} \tag{13}$$

$$\begin{bmatrix} G_{11}=\dfrac{10^4\times\left(5.25s^4+56.99s^3+181.8s^2+145s+10.11\right)}{s^5+376.9s^4+3995s^3+12710s^2+10610s+109.9} & G_{12}=\dfrac{-77.7s^3-762s^2-943.6s-68.18}{s^5+376.9s^4+3995s^3+12710s^2+10610s+109.9} \\ G_{21}=\dfrac{10^4\times\left(1.141s^3+38.62s^2+257.1s+19.57\right)}{s^5+376.9s^4+3995s^3+12710s^2+10610s+109.9} & G_{22}=\dfrac{17.7s^3+6486s^2+8868s-22.04}{s^5+376.9s^4+3995s^3+12710s^2+10610s+109.9} \end{bmatrix} \tag{14}$$

Based on the multi-model approach, the triangle membership function, schematically shown in Fig. 2, is used for the fuzzy weighting of the transfer function models at the five power levels to establish the reactor core multi-model system that is applicable to the entire operational condition. The mathematical description of the multi-model is given by Eq. (15).where M_i denotes the weighting coefficient of the i-th local model.

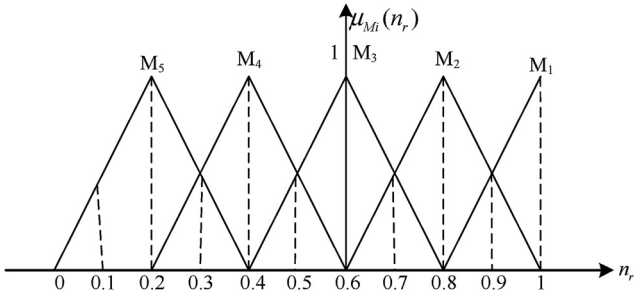

Fig. 2. Membership curves of the local core models.

$$G_r(s)=\sum_{i=1}^{5} M_i G_{ri}(s) \tag{15}$$

3. Robust reactor power control system design

Since the small PWR in the present study is expected to operate with large external disturbances and internal uncertainties, a robust power control system should be designed to ensure the stable operation of the reactor. Considering the effectiveness and efficiency of the H_∞ mixed sensitivity to realize robust control of a complex system with various uncertainties [22,23], it is employed to design the robust power control system for the small PWR here.

3.1. H_∞ mixed sensitivity control theory

The H_∞ mixed sensitivity robust control method is applied for the robust power controller design for the small PWR. Since the robust stability and the resistance to external disturbances are the most important performance indexes for the closed-loop reactor power control system, they are taken into consideration in the mixed sensitivity design here.

3.1.1. Sensitivity and complementary sensitivity

The structure of a common mixed sensitivity design model is schematically shown in Fig. 3. Here, $r(t)$ is the reference input; $e(t)$ is the tracking error; $u(t)$ is the control input; $d(t)$ is the

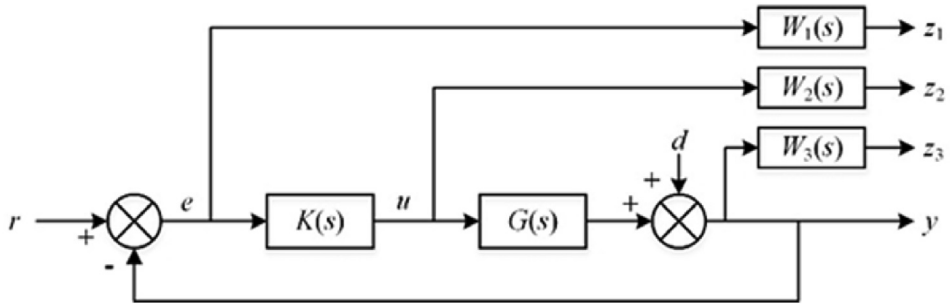

Fig. 3. Weighing mixed sensitivity design model.

disturbance; $y(t)$ is the system output;$K(s)$ is the controller; $G(s)$ is the controlled object model. The weight functions $e(t)$, $u(t)$ and $y(t)$ are expressed as $W_1(s)$, $W_2(s)$ and $W_3(s)$, respectively [24]; z_1, z_2 and z_3 are the signals for the system evaluation.

The closed-loop transfer functions from the $r(t)$ to the $e(t)$, $u(t)$ and $y(t)$ can be, respectively, expressed as

$$S(s) = [I + G(s)K(s)]^{-1} \tag{16}$$

$$R(s) = K(s)[I + G(s)K(s)]^{-1} = K(s)S(s) \tag{17}$$

$$T(s) = G(s)K(s)[I + G(s)K(s)]^{-1} = I - S(s) \tag{18}$$

where $S(s)$ is the sensitivity function; $R(s)$ is the control sensitivity function; $T(s)$ is the complementary sensitivity function.

The closed-loop transfer functions from the $r(t)$ to the z_1, z_2 and z_3 can be given by

$$\begin{aligned}\Phi(s) &= \begin{bmatrix} W_1(s)S(s) \\ W_2(s)R(S) \\ W_3(s)T(s) \end{bmatrix} \\ &= \begin{bmatrix} W_1(s)[I + G(s)K(s)]^{-1} \\ W_2(s)K(s)[I + G(s)K(s)]^{-1} \\ W_3(s)G(s)K(s)[I + G(s)K(s)]^{-1} \end{bmatrix} \\ &= \begin{bmatrix} W_1(s) \\ 0 \\ 0 \end{bmatrix} + \begin{bmatrix} -W_1(s)G(s) \\ W_2(s) \\ W_3(s)G(s) \end{bmatrix} K(s)[I + G(s)K(s)]^{-1}\end{aligned} \tag{19}$$

The mixed sensitivity problems can be translated to find a rational function controller $K(s)$ to make the closed-loop system stable and to minimize the H_∞ norm of the $\Phi(s)$, namely [25].

$$\|\Phi\|_\infty = \left\| \begin{matrix} W_1(s)S(s) \\ W_2(s)R(s) \\ W_3(s)T(s) \end{matrix} \right\|_\infty \le 1 \tag{20}$$

Eq. (20) can be transformed into the following inequalities.

$$\begin{cases} \|S\|_\infty \le \left\|W_1^{-1}\right\|_\infty \\ \|R\|_\infty \le \left\|W_2^{-1}\right\|_\infty \\ \|T\|_\infty \le \left\|W_3^{-1}\right\|_\infty \end{cases} \tag{21}$$

According to Eq. (21), the satisfactory $S(s)$, $R(s)$ and $T(s)$ can be obtained by choosing appropriate weighting functions $W_1(s)$, $W_2(s)$ and $W_3(s)$.

3.1.2. Weight functions selection

The H_∞ robust control theory is perfect both in the basic theory and algorithm, except for the selection of the weight functions for different control objects and targets. Since there are no specific rules to follow, the determination of the three weight functions mostly depends on the designers' experience. In general, the order of a weight function should not be too high.

$W_1(s)$ is the weight function of $S(s)$, which means the constraints of the system performance requirements to reflect the sensitivity features. $W_1(s)$ can be regulated to restrain the interference effectively and to get the desired output. At low frequencies, with the increase in the gain value of $W_1(s)$, the reference tracking performance of the closed-loop system increases and the disturbance influence decreases. The overshoot is controlled at high frequencies. Therefore, $W_1(s)$ is generally designed to possess the integral, high gain and low-pass characteristics. $W_1(s)$ can be written in a standard form as

$$W_1 = \frac{K_1}{T_1 s + b_1} \tag{22}$$

$W_3(s)$ is the weight function of $T(s)$, which represents the multiplicative perturbation norm boundary and reflects the robust stability requirements. Since high-frequency unmodeled dynamic characteristics and measurement noises in the low frequencies are relatively small, a higher amplitude $W_3(s)$ are selected to suppress high frequency measurement noises, which can be formulated as

$$W_3 = \frac{K_3 s}{T_3 s + b_3} \tag{23}$$

$W_2(s)$ is the weight function of $R(s)$,which reflects the limitation on additive uncertainties and guarantees stability of the designed controller. $W_2(s)$ can be obtained after the selections of $W_1(s)$ and $W_3(s)$ [26]. Generally, $W_2(s)$ is a small constant.

3.2. H_∞ robust power controller design

Block diagram of the small PWR power control system is shown in Fig. 4. The reactor core model has two inputs and two outputs. The inputs are the reactivity introduced by control rods and the coolant inlet temperature of the reactor core, and the outputs are the coolant outlet temperature and reactor power. During power maneuvers of the reactor, only the reactivity introduced by control rods can be controlled by regulating their positions in the core. According to the coolant temperature operational scheme, the reactor power and coolant outlet temperature can be both maintained by controlling either of them. In the present study, the reactor power is chosen as the controlled variable. The error between the actual reactor power and its reference value is sent to the power controller as an input.

In Fig. 4, G_{ci} is the reactor power controller to be designed; K_c is the transfer function of the control rod drive mechanism, which is simplified as an integral term expressed as $K_c = 1/s$; K_r is the

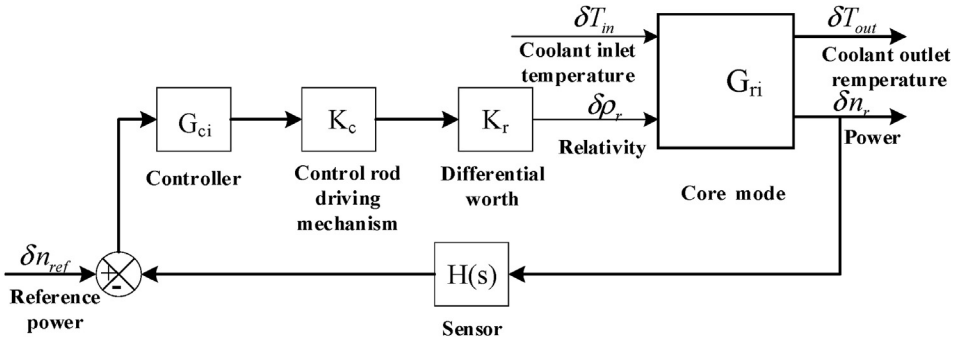

Fig. 4. Block diagram of the reactor power control system.

Table 1
wt coefficients at the five power levels.

Power level	W_1	W_2	W_3
100%FP	$\frac{0.3}{50s+0.1}$	0.001	$\frac{s}{s+100}$
80%FP	$\frac{0.32}{60s+0.13}$	0.001	$\frac{1.3s}{2s+100}$
60%FP	$\frac{0.38}{80s+0.15}$	0.0001	$\frac{1.6s}{4s+100}$
40%FP	$\frac{0.42}{100s+0.16}$	0.0001	$\frac{2s}{7s+100}$
20%FP	$\frac{0.45}{120s+0.18}$	0.00001	$\frac{2.5s}{10s+100}$

control rod differential worth ranging from 3 pcm/step to 12 pcm/step; $H(s)$ is the transfer function of nuclear power measuring equipment which can be expressed as $H(s)=1/(s+1)$.

In H infinity controller designs, the design specifications are usually converted to appropriate weighting coefficients, and there are some methods on the design of specific weighting coefficients. In order to eliminate the steady-state error in the closed-loop system and reject constant load disturbances, $S(s)$ should be small in the low frequency region. For $T(s)$, the robust stability requirement should be considered first to resist the large model uncertainty in low frequency region, While in high frequency region, $T(s)$ should prevent the closed-loop system becoming too sensitive to high frequency noises. The magnitude of $R(s)$ relates to the actuator efforts. In general, the practical considerations or physical limitation of control actuators place a bound on the magnitude of $R(s)$. Based on the above guidelines and the desired expectation, the weighting coefficients could be designed in iterative and trial-and-error manners to satisfy the uncertainty bound and the physical limitations on the reactor core power change. The weighting functions for the H_∞ mixed sensitivity design here at the five power levels are given in Table 1.

With these weighting functions in Table 1, five local H_∞ robust power controllers were designed for the small PWR using the robust control toolbox in MATLAB [27], which are given in Table 2 above.

The singular value Bode plots of $S(s)$ and $1/W_1(s)$ at the five power levels are presented in Fig. 5, and those of $T(s)$ and $1/W_3(s)$ are shown in Fig. 6. From Figs. 5 and 6, it is clear that the singular values of the sensitivity function $S(s)$ and the complementary sensitivity function $T(s)$ are smaller than those of the $1/W_1(s)$ and $1/W_3(s)$, satisfying the selection principle of the weighting functions. In low frequencies, the singular values of $S(s)$ is very small, indicating the closed-loop control system has good disturbance attenuation capability and is insensitivity to the parameter perturbation of the reactor. In high frequencies, the larger singular value of $T(s)$ than that of $1/W_3(s)$ indicates the designed controller is capable of suppressing high-frequency unmodeled dynamics of the system. Therefore, the weight coefficients are selected reasonably, and the designed control system has strong robustness.

3.3. Multi-model power control system

Each of the H_∞ robust power controllers in Table 2 is designed based on the linearized reactor core model at a particular equilibrium condition, which is expected to have satisfactory control performance only in a small range around the equilibrium condition. So the multi-model approach is applied to synthesize the five robust controllers into a multi-model robust power control system for the small PWR with the multi-model controller given by

$$G_{c,m}(s)=\sum_{i=1}^{5} M_i G_{c,i}(s) \tag{24}$$

where $G_{c,m}$ is the multi-model robust power controller; the weighting coefficient M_i for the i-th robust power controller can be

Table 2
H_∞ robust power controllers at the five power levels.

Power level	Controller transfer functions
100%FP	$G_{c1}=\frac{9.5788(s+365.9)(s+100)(s+5.712)(s+0.03427)(s^2+5.35s+8.083)}{(s+1.575\times10^8)(s+5.263)(s+4.516)(s+1.571)(s+1.12)(s+0.07702)(s+0.002)}$
80%FP	$G_{c2}=\frac{8.4971(s+366)(s+50)(s+5.639)(s+0.03002)(s^2+5.367s+7.454)}{(s+1.024\times10^8)(s+5.265)(s+4.492)(s+1.293)(s+1.12)(s+0.07698)(s+0.002167)}$
60%FP	$G_{c3}=\frac{75.543(s+366)(s+25)(s+5.58)(s+3.388)(s+1.999)(s+0.02489)}{(s+6.3\times10^8)(s+5.254)(s+4.507)(s+1.11)(s+1.092)(s+0.07703)(s+0.001875)}$
40%FP	$G_{c4}=\frac{66.668(s+366)(s+14.29)(s+5.487)(s+3.821)(s+1.582)(s+0.01854)}{(s+4.5\times10^8)(s+5.23)(s+4.508)(s+1.09)(s+0.9111)(s+0.07704)(s+0.0016)}$
20%FP	$G_{c5}=\frac{5.9427(s+366.1)(s+10)(s+5.378)(s+4.146)(s+1.283)(s+0.01049)}{(s+3.937\times10^7)(s+5.257)(s+4.455)(s+1.068)(s+0.7659)(s+0.07698)(s+0.001481)}$

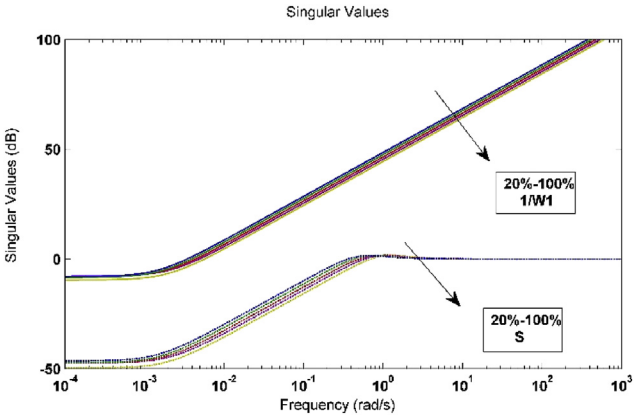

Fig. 5. Singular value Bode plots of $S(s)$ and $1/W_1(s)$.

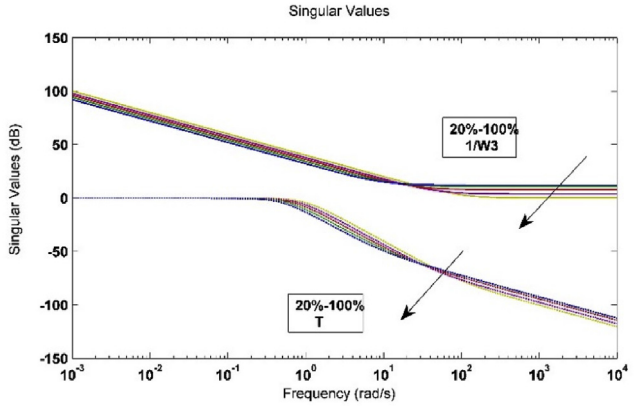

Fig. 6. Singular value Bode plots of $T(s)$ and $1/W_3(s)$.

calculated according to the triangle membership functions presented in Fig. 2.

4. Results and discussion

4.1. Controller performance assessment

The phase margins and magnitude margins of the open loop control system in Table 3, at the five power levels, are calculated and tabulated in Table 3. The results indicate that all the phase margins are larger than 60 deg and the amplitude margin are all infinity for the five cases, indicating the designed H_∞ robust power controllers can provide good performance in terms of stability.

When the reference input δn_r is increased by 0.1, the step responses of the closed-loop reactor power control system at the five power levels are shown in Fig. 7. It is clear that the designed controllers can ensure good reference tracking performances of the

Table 3
Phase margins and magnitude margins of the open loop reactor power control system.

Power levels	Phase margin (deg)	Magnitude margin (dB)
100%(FP)	70.5	∞
80%(FP)	70.7	∞
60%(FP)	70.8	∞
40%(FP)	71	∞
20%(FP)	71.2	∞

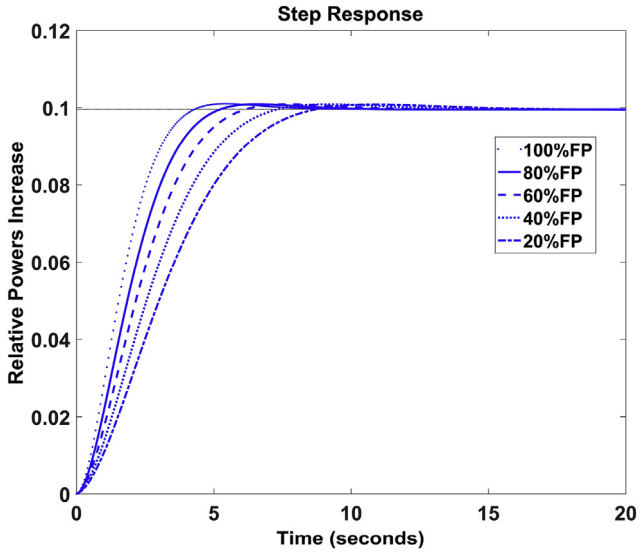

Fig. 7. Step responses of the closed-loop reactor power control system at the five power levels.

closed-loop reactor power control system in terms of small overshoots and short settling times.

4.2. Multi-model control simulation and analysis

A multi-model control simulation platform is developed in MATLAB/Simulink environment with implementation of the reactor core multi-model system presented in Section 1 and the multi-model power control system designed in Section 3. Block diagram of the simulation platform in Simulink is shown in Fig. 8, where the coolant inlet temperature perturbation denoted by δT_{in} can be taken as an external disturbance on the reactor core system.

Based on the simulation platform, two kinds of typical operational transients of the small PWR are simulated with the simulation conditions defined by the following two cases:

CASE A: A 10% FP step increase in the reference power is introduced to the reactor core system at the beginning of the simulation first, then a 0.5 °C increase in the coolant inlet temperature happens at 100s, and the total simulation time is 200s.

CASE B: The reactor operates at 100%FP initially. At t = 345s, the reference power decreases at the rate of 5%FP/min to 30%FP, and then keeps constant till t = 1815s when it begins to increase to the 100%FP again at 2655s.

Dynamic simulations of the small PWR with the Case A transient introduced at the five power levels have been performed, respectively, and the simulation results are presented in Fig. 9. It can be seen that, for all the five power levels, the reactor power tracks its reference value very well with the settling time shorter than 10s and the overshoot smaller than 1% when a 10% step increase happen on the reference power at the beginning of the transient. This demonstrates the designed control system have good reference tracking capability. Moreover, when a 0.5 °C increase happens on the coolant inlet temperature, the reactor power decreases rapidly first due to the negative temperature feedback of the coolant, and then it can be regulated to follow the reference power rapidly with control actions for all the five power levels. Since the coolant inlet temperature perturbation can be taken as a disturbance to the closed-loop reactor power control system, it can be drawn that the design multi-model control system has good disturbance rejection capability.

Dynamic response of the rector power during the Case B

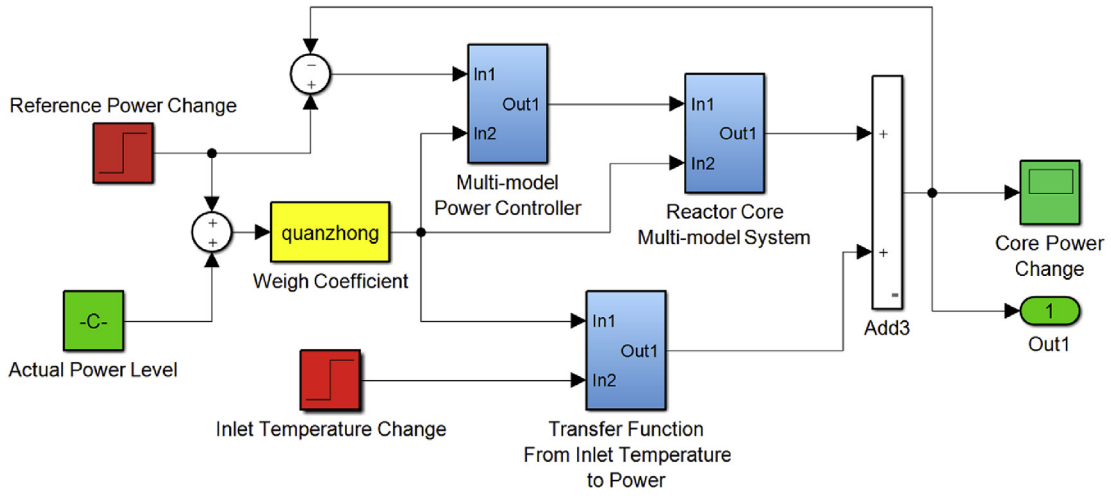

Fig. 8. Block diagram of the Multi-model control system platform in Simulink.

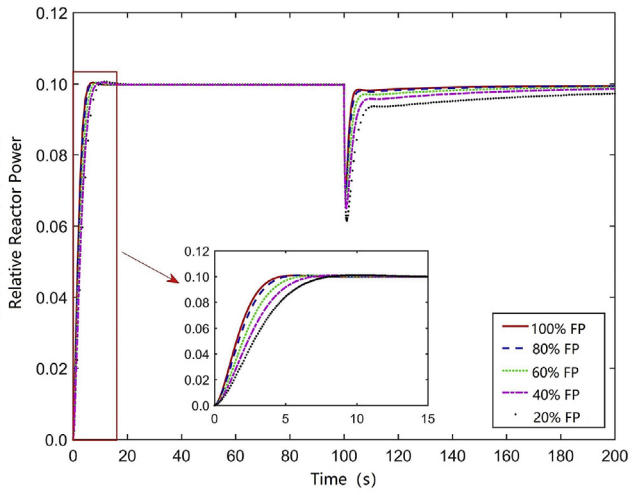

Fig. 9. Dynamic responses of the reactor power during the CASE A transients at the five power levels.

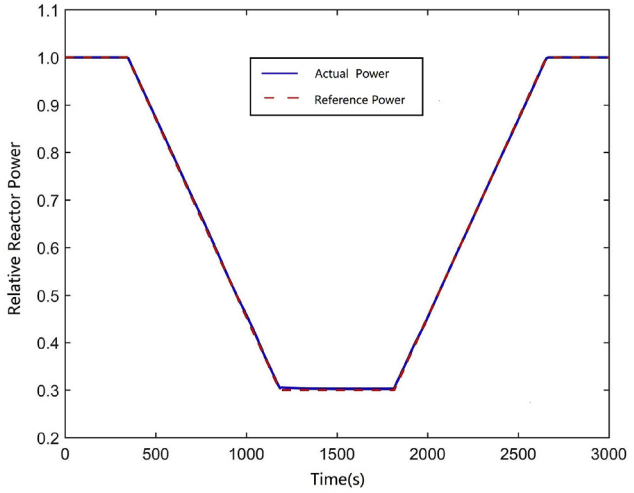

Fig. 10. Dynamic responses of the reactor power during the CASE B transient.

transient is presented in Fig. 10. It is clear that the reactor power follows its reference value very well at both the 5% FP/min ramp load decrease and increase processes between 30% FP and 100% FP. This demonstrates that the designed multi-model power control system has good control performance over a wide power range.

5. Conclusion

Considering the model uncertainty and external interference during operations of the small PWR, the multi-model system of the reactor core is established with integration of transfer function core models at five typical power levels by using the weighted multi-model approach, and then the multi-model robust power control system of the reactor core is designed by using the robust H_∞ mixed sensitivity method. On this basis, a multi-model robust control simulation platform is developed in MATLAB/Simulink for transient simulation studies of the small PWR. The simulation results of the reactor, during the transient with a 10% FP step increase in the reference power first and a 0.5 °C increase in the coolant inlet temperature after that for all the five power-levels, have demonstrated the good reference tracking and disturbance rejection performances of the designed multi-model robust power control system. Moreover, the good load follow performance of the reactor during the 5% FP/min ramp load change transient illustrates the effectiveness of the multi-model control system during transient operations over wide power ranges. It can be drawn from the simulation and analysis results that the designed multi-model robust power control system have excellent control performance and good robustness, and the H_∞ hybrid sensitivity based robust control method in the present study is applicable to the power control design of small PWRs with strong external disturbances and model uncertainties.

Declaration of competing interest

No conflict of interest.

Acknowledgment

This research is funded by the National Natural Science Foundation of China (Grant No. 11805147) and the China Postdoctoral Science Foundation (Grant No. 2018T111068).

Appendix A. Supplementary data

Supplementary data to this article can be found online at https://doi.org/10.1016/j.net.2019.12.031.

References

[1] J. Yang, J.L. Sun, W.G. Yang, R. Shu, ACPR100 concept design of multipurpose compact Reactor, Atomic Energy Sci. Technol. 48 (2014) 1844–1849.
[2] W.M. Stacey, Nuclear Reactor Physics, John Wiley & Sons, 2007, pp. 162–167.
[3] L. Liu, X.C. Luan, S. Rao, G.Y. Jin, Y.U. Tao, Application of fuzzy robust control method in power control of nuclear reactors, Atomic Energy Sci. Technol. 47 (2013) 624–629.
[4] W.Y. Wu, Design and Simulation of Reactor Power Controller Based on QFT Theory, North China Electric Power University, Beijing (China), 2013 (In Chinese).
[5] G. Li, F.Y. Zhao, Flexibility control and simulation with multi-model and LQG/LTR design for PWR core load following operation, Ann. Nucl. Energy 56 (2013) 179–188.
[6] G. Li, Modeling and LQG/LTR control for power and axial power difference of load-follow PWR core, Ann. Nucl. Energy 68 (2014) 193–203.
[7] G.R. Ansarifar, H.R. Akhavan, Robust nonlinear control for nuclear reactors using sliding mode observer to estimate the xenon concentration, Nucl. Sci. Technol. 27 (2016) 28.
[8] L.T. Liao, P.F. Wang, Study of multi-model internal model robust control for a small pressurized water reactor core, Autom. Instrum. 33 (2018) 76–94.
[9] M. Zaidabadi nejad, G.R. Ansarifar, Robust feedback-linearization control for axial power distribution in pressurized water reactors during load-following operation, Nucl. Engineering. Technol. 50 (2018) 97–106.
[10] S.M.H. Mousakazemi, N. Ayoobian, Robust tuned PID controller with PSO based on two-point kinetic model and adaptive disturbance rejection for a PWR-Type reactor, Prog. Nucl. Energy 111 (2019) 183–194.
[11] P.F. Fan, Y.H. Fan, Y.F. Yu, Hybrid sensitivity control for air-launched cruise missile hinfinity, Comput. Mod. 7 (2013) 105–108.
[12] K. Suzuki, J. Shimazaki, Y. Shinohara, Application of H control theory to power control of a nonlinear reactor model, Nucl. Sci. Eng. 115 (1993) 241–251.
[13] S. Chi, N.Z. Cho, H_∞ control theory applied to xenon control for load-following operation of a nuclear reactor, Nucl. Technol. 137 (2002) 127–138.
[14] J. Sun, G. Xia, F. Sun, Application of H infinity control method in power control of nuclear reactors, Appl. Technol. 32 (2005) 46–48 (In Chinese).
[15] B.E. Sedhom, A.Y. Hatata, M.M. El-Saadawi, H.E. Abd-Raboh, Robust adaptive H-infinity based controller for islanded microgrid supplying non-linear and unbalanced loads, IET Smart Grid 2 (2019) 420–435.
[16] R. Gerasimos, S. Pierluigi, A. Sul, Nonlinear H-infinity control for switched reluctance machines, Nonlinear Eng. 9 (2020) 14–27.
[17] S.V. Madhavi, G.T.R. Das, A robust H-infinity controller for an isolated boost converter used in fuel cell application, J. Electric. Syst. 15–2 (2019) 197–212.
[18] B. Zhou, S. Xie, J. Hui, H-infinity control for T-S aero-engine wireless networked system with scheduling, IEEE Access 7 (2019) 115662–115672.
[19] M.Z.M. Tumari, A.S.R.A. Subki, M.S.M. Aras, M.A. Kasno, M.A. Ahmad, M.H. Suid, H-infinity controller with graphical LMI region profile for liquid slosh suppression, Telkomnika 17 (5) (2019) 2636–2642.
[20] T.W. Kerlin, E.M. Katz, J.G. Thakkar, Theoretical and experimental dynamic analysis of the HB Robinson nuclear plant, Nucl. Technol. 30 (1976) 299–316.
[21] J.S. Wan, P.F. Wang, S.F. Wu, F.Y. Zhao, Controller design and optimization of reactor power control system for ASPWR, Prog. Nucl. Energy 100 (2017) 233–244.
[22] D. Lee, K.S. Kim, S. Kim, Controller Design of an electric power steering system, IEEE Trans. Control Syst. Technol. 26 (2018) 748–755.
[23] C.T. Faria, G. Pulvirenti, T. Geluk, Modeling and nonlinear parameter identification of an electric-power steering system, in: Proceedings of the Society for Experimental Mechanics Series Conference, Springer, Cham, 2017.
[24] W.Z. Zhao, Y.J. Li, C.Y. Wang, Z.Q. Zhang, C.L. Xu, Research on control strategy for differential steering system based on H_∞ hybrid sensitivity, Int. J. Automot. Technol. 14 (2013) 913–919.
[25] J.C. Doyle, K. Glover, P.P. Khargonekar, B.A. Francis, State-space solution to standard H_2 and H_∞ control problems, IEEE Trans. Autom. Control (1989) 831–847.
[26] P. Wang, H.C. Liao, Z.X. Deng, Study on the mixed sensitivity control of H infinity damping in the alert constraint layer, J. Vib. Shock 35 (2016) 168–173 (In Chinese).
[27] R.C. Dorf, R.H. Bishop, Modern Control Systems, Publishing House of Electronics Industry, Beijing (China), 2005.